Morphological and optical characterization of self-assembled InAlGaAs/GaAs quantum dots

Seunghyun Lee, Riazul Arefin, Hyemin Jung, et al.

View Online   Export Citation   CrossMark

AIP Publishing

Morphological and optical characterization of self-assembled InAlGaAs/GaAs quantum dots

View Online   Export Citation   CrossMark

Seunghyun Lee,[1] [ID] Riazul Arefin,[1] [ID] Hyemin Jung,[1] Jaedu Ha,[2] Md Saiful Islam Sumon,[1] Jong Su Kim,[2] [ID] Sanjay Krishna,[1] [ID] and Shamsul Arafin[1,a)] [ID]

AFFILIATIONS

[1]Department of Electrical and Computer Engineering, The Ohio State University, Columbus, Ohio 43210, USA
[2]Department of Physics, Yeungnam University, Gyeongsan 38541, South Korea

a)Author to whom correspondence should be addressed: arafin.1@osu.edu

ABSTRACT

This experimental study reports the morphological and optical properties of self-organized quaternary InAlGaAs quantum dots (QDs) grown on GaAs substrates. Atomic force microscopy (AFM) revealed the presence of QDs and their geometry across the sample surface, while the optical properties were verified by photoluminescence (PL) spectroscopy. Temperature-dependent PL measurements were performed for a series of samples with different indium compositions. Unlike conventional quantum well materials, the change in PL peak positions in QD structures exhibits a non-monotonic exotic dependence on temperature. Our AFM data confirm a bimodal distribution of dot sizes as corroborated by calculated thermal activation energies. A rapid decrease in the PL signal at elevated temperatures suggests that thermionic emission and interface defects are the two dominant mechanisms of carrier escape and recombination in these QD structures. Such a quaternary QD-based active region is important for realizing next-generation diode lasers with an emission wavelength shorter than $1\,\mu$m.

INTRODUCTION

Over the past few decades, research in semiconductor quantum dots (QDs) has garnered much interest in a wide range of both classical-[1–3] and quantum-emitters.[4] Owing to three-dimensional (3D) carrier confinement and atom-like discrete density of states, QD-based active regions, especially in semiconductor diode lasers, provide numerous benefits, such as enhanced thermal-stability,[5] insensitivity to back-reflection,[6] lower threshold current density,[2] and ultra-narrow spectral linewidth.[7] All these appealing advantages can only be obtained once the QDs' uniformity in terms of size, shape, and composition is maintained and a high surface density of QDs is achieved.

There has been extensive research on InAs/GaAs[6,8] and InAs/InAlGaAs/InP[9,10] QDs for devices at telecom and datacom wavelengths. Devices emitting at shorter than $1\,\mu$m are also important for a wide range of emerging applications, including topographic LiDAR,[11] solid-state and fiber-amplifier pumping,[12] therapeutics,[13] and heat-assisted magnetic recording.[14] Although deploying standard quantum well lasers to those applications is a long practice, QD-based lasers emitting this wavelength range are expected to

drastically improve the device performance, being useful for these applications with advanced operations.

Since 1996, ternary AlInAs[15] and quaternary $Al_xGa_yIn_{1-x-y}As$[12] QDs were found to be promising candidates for accessing this short wavelength regime. In particular, AlGaInAs QDs are more attractive since this material platform allows adjusting of strain and emission wavelength in a wide range by varying In and Al contents in addition to achieving high QD density, yielding QD edge-emitting[12,16] and vertical-cavity[17] lasers at <1 μm. However, the presence of Al and its high surface binding energy or low surface migration length led to spatial inhomogeneity of localized strain, compositions, and QD geometry,[18,19] bringing new challenges to investigate their optical properties.

Hence, a comprehensive study on the surface morphology and optical properties of self-assembled AlGaInAs QDs is of primary interest prior to their use in realizing high-performance diode lasers.[20] Prior studies reported the bimodal distribution of QDs due to variations in strain across the growth surface creating severe non-uniformity in QD dimensions.[21,22] Carrier thermal escape and transfer due to QD size variation were also reported.[23] Eventually,

all these effects attributed to the optical characteristics of the QDs and deviation from typical features of defect-free uniform QD ensemble is discernible.

As the spatial and compositional variations significantly affect the optical and electronic performance of the QDs, a detailed study of temperature-dependent carrier redistribution and repopulation mechanisms of this class of nanostructures aid optimize material growth conditions. This will eventually help toward realizing thermally-stable lasers.[18,24,25] In this article, we investigated the carrier recombination mechanism caused by compositional fluctuations in AlGaInAs QDs by temperature-dependent photoluminescence (TDPL) measurements. Due to varying localized strain and compositions, a bimodal distribution is found in QD morphology. Non-monotonic and exotic temperature-dependent emission properties are observed in photoluminescence (PL) peak locations vs temperature. The reason for the exotic temperature behavior within an ensemble of QDs is also explained by PL FWHM and integrated PL intensity as a function of temperature. Finally, the QD carrier repopulation mechanism and drastic reduction in the PL signal with increasing temperature were also discussed.

EXPERIMENTAL DETAILS

Self-assembled InAlGaAs/GaAs QDs were grown in a solid source molecular beam epitaxy (MBE) using a RIBER compact 21DZ reactor. The most popular growth technique known as Stranski–Krastanov (S-K) was employed to grow QD samples. Prior to QD growth, the growth rates of Al, Ga, and In were calibrated by RHEED and chosen to be 0.5, 1, and $0.2\,\mu$m/h, respectively. The epitaxial growth started with depositing a 300-nm-thick GaAs buffer layer on top of semi-insulating GaAs (100) substrates at 600 °C. Quaternary active QDs were then grown at a temperature of 520 °C by the so-called "digital alloy" technique where $Al_{0.71}In_{0.29}As$, $Ga_{0.83}In_{0.17}As$, and InAs were deposited in two cycles. During the deposition of InGaAs, AlInAs, and InAs, V/III ratios were adjusted to 10, 20, and 40, respectively. 4.9 monolayers (MLs) of QD materials was deposited for the onset of 3D transition.[16] After deposition of each cycle, the group-III flux is deliberately interrupted for 10 s to enhance surface migration and promote QD formation.[18] The QDs were embedded in a 300-nm-thick GaAs barrier layer grown at 600 °C. The growth ended with an identical QD layer on top of the barrier for the assessment of QD morphology. Figure 1 schematically shows the representative QD samples used in this study.

Indium-content is one of the most eminent variational parameters for QDs to control emission wavelengths.[12,16] Therefore, three different PL samples with $In_xAl_{0.15}Ga_{0.85-x}As$ QDs were grown where $x = 0.62$, 0.52, and 0.42, while the Al composition was kept constant at 15%. Morphological analyses were performed in a Bruker Dimension Icon AFM. The use of an NSC15 cantilever with a diameter of 16 nm provided an accurate measurement of QD height, but diameter measurement was affected owing to tip deconvolution and high density of QDs.[26] Optical properties of the PL structures were measured using a continuous-wave 405 nm laser with a constant pump intensity of $0.6\,W/cm^2$. Temperature-dependent PL was performed on QD samples using a photomultiplier tube (PMT) in the temperature range of 20–300 K.
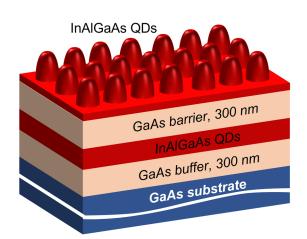

FIG. 1. Schematic cross-sectional view of test structures with identical embedded and surface QD layers for structural and optical characterization.

RESULTS AND DISCUSSION

Figure 2 shows the 3D AFM images of the three InAlGaAs QD samples. Bimodal distributions of QDs with two different families are observed for 62%, and 52% In-containing samples. Small and big QDs are marked by red- and green-colored dashed circles in Figs. 2(a) and 2(b), respectively. Surface roughness in the range of only 1 nm is obtained for the 42% In-containing sample, suggesting a 2D-like growth mode as shown in Fig. 2(c). As the critical thickness required for the emergence of 3D growth mode transition is higher than the thickness of the deposited QD layer in the 42% In-containing sample, planar growth is favored with identical growth conditions.[16] Importantly, the 62% In containing sample exhibits relatively smaller QDs compared to 52% In-containing ones. The AFM image of the 52% In containing sample confirms the reduced density of the 3D islands due to a low In-content.[27]

The QD size histograms of 62% and 52% In-containing samples are shown in Figs. 2(d)–2(g). In particular, the height and diameter distributions of the QDs are presented for each sample. Both the samples show bimodal distributions of dots represented by a Gaussian probability distribution function. In fact, the histograms of dot height and base diameter for samples were best fitted with two Gaussian distributions of mean and standard deviations. The mean values along with the standard deviations as well as QD densities are listed in Table I.

Figures 3(a)–3(c) show the TDPL spectra of the three samples. No emission from the wetting layer is observed, which indicates that the carriers photogenerated in these layers rapidly transported to QDs and afterward recombine from there. At 20 K, the measured PL peaks are centered at 1.33, 1.32, and 1.36 eV for 62%, 52%, and 42% In-containing samples, respectively. The electronic band diagram of QDs was then calculated by employing the 6-band $k.p$ model[28] and extracting the QD geometry information from the AFM data in Fig. 2. Considering the QD geometry and the ground states of $In_xAlGaAs$ with $x = 0.62$ and 0.52, the calculated photon energies are 1.33 and 1.32 eV, respectively, showing a complete agreement with the measured data.
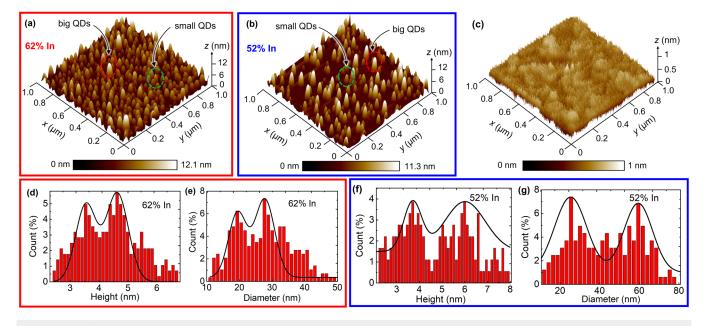
FIG. 2. $1 \times 1 \, \mu m^2$ AFM images of $In_xAl_{0.15}Ga_{0.85-x}As$ QD samples with different indium contents: $x =$ (a) 0.62, (b) 0.52, and (c) 0.42. Height and diameter histograms for bimodally distributed QDs for samples with In-contents of (d) and (e) 62% and (f) and (g) 52%.

The presence of high binding energy of Al yields a reduced migration length of In adatoms on GaAs (100) surfaces and smaller dot sizes are formed. Hence, this causes spatial size inhomogeneities in QDs, which subsequently influence the carrier recombination mechanism.[18,29,30] This is understood by the "red–red–constant" exotic temperature dependence of PL peak emission wavelengths, as shown in Figs. 3(a) and 3(b). In particular, an initial mild red shift of the emission wavelength followed by a rapid red shift and finally a constant PL peak position with increasing temperature was observed in our experiment. The distinguishable PL-emission peaks are seen from 20 to 220 K for 62% and 52% In-containing samples, suggesting a strong 3D confinement of carriers. A noticeable drop of the PL signal is observed at a temperature of >140 K for the 42% In sample as shown in Figs. 3(c), which is a consequence of QD growth being suppressed with strain and thickness below the critical value, leading to 1D

carrier confinement within a thin layer. Different QD families with varying dot sizes can be obtained for multi-dispersed and broader QD ensembles.[31] The PL spectra of the overall QD ensemble are dominated by different QD families at different temperatures. This behavior is particularly more interesting for InAlGaAs QDs as the presence of Al and its high binding energy has direct consequence on QD size distribution. This makes our quaternary QD system distinct from the well-studied InAs/GaAs[24,32] and InAs/InP[33,34] QD systems.

To distinguish the individual contribution of each QD family, the measured PL spectrum at a given temperature was deconvoluted by two Gaussian bands at three representative regions of temperature, i.e., 20, 140, and 180 K. Each Gaussian function corresponds to a certain QD family. Figures 3(d) and 3(e) show the Gaussian bands for both 62% and 52% In-containing samples, respectively. The smaller QDs are expected to provide higher energy emission, whereas the low-energy emission is obtained from the big QD family.

At the low-temperature regime around 20 K, the integrated PL intensity contributed by the big QD family is higher than that of the small one, as can be seen in Figs. 3(d) and 3(e) for 62% and 52% samples, respectively. We attribute this phenomenon primarily to higher carrier occupation in big QDs where a higher radiative recombination rate is expected compared to small QDs. This was also verified by calculating the electron–hole wavefunction overlap for big and small QDs of the 62% In-content sample. The calculated overlaps for big and small QDs are 1.3 and 0.88, respectively. A factor of ~1.5 higher overlap was also calculated from the big QDs vs small QDs in the 52% In sample. Moreover, the slightly higher or even equal dot density of the big family with respect to

TABLE I. Morphology of the Bi-modally distributed QDs of 62% and 52% indium compositions.

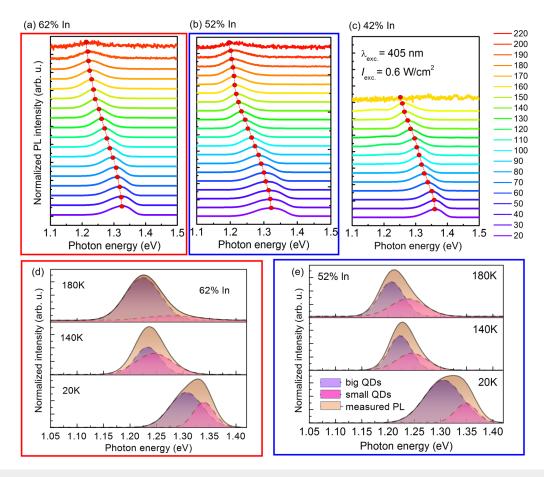| In content	Large QD family		Small QD family		Density (cm^{-2})
	Mean height	Mean diameter	Mean height	Mean diameter	
62%	5 nm (±0.57)	30 nm (±5)	3.1 nm (±0.4)	20 nm (±3.4)	5×10^{10}
52%	6.6 nm (±0.58)	67 nm (±20)	3.6 nm (±0.5)	24 nm (±5.5)	2×10^{10}

FIG. 3. Temperature-dependent PL characteristics of InAlGaAs QDs with indium contents of (a) 62%, (b) 52%, and (c) 42%; numbers in legend indicate temperature in Kelvin. Deconvolution of PL spectra at three representative regions for only (d) 62% and (e) 52% indium-content samples.

the small one [see the histograms in Figs. 2(d)–2(g)] partly explains the higher integrated PL intensity contributed by the big QD family.

After deconvoluting the spectra at an intermediate temperature of 140 K, identical contributions from the big- and small-QD families of each sample are noticed. We presume that this behavior is due to thermionic emission of carriers that were homogeneously distributed across the entire QD ensemble at low temperatures. With increasing temperature, thermalized carriers continue to populate the nearby QDs. As the QDs are distributed in a bi-Gaussian shape, this carrier population mechanism is faster for dominant QD families. As a result, the contribution to optical emission from both QD families comes closer in the intermediate temperature range.

At high temperatures, e.g., 180 K, different behavior is seen from the deconvoluted spectra of big and small QD families. For the 62% sample, it is seen that most of the contribution are coming from the big QD family. This could be due to the transfer of thermalized carriers from the small-to-big QD family. On the contrary, a reasonable contribution, roughly 40%, is coming from the small

QD family of the 52% sample. This could be explained by the availability of small QDs with a larger dimension in the 52% sample as can be seen in Table I and the AFM images in Fig. 2. That is, the mean diameter and height of the small QDs appear larger in the 52% sample than the 62% one. Therefore, compared to the 62% sample, the thermal carrier transfer process in the 52% one becomes slower at higher temperatures.

The temperature dependence of PL peak positions for the QD samples was then analyzed. Figure 4(a) shows the measured PL temperature range, which is divided into three distinct regions and marked as regions 1, 2, and 3. In region-1, a slight red shift with a weak temperature dependence of PL peak energy is observed. At a low temperature range, the PL transition energy is determined by the inhomogeneous distribution of the QD ensemble where the carriers are homogeneously distributed across all QDs of different sizes and shapes as stated earlier. More specifically, the ground state energies of the entire QD ensemble composed of QDs with different sizes and shapes are responsible for optical transitions. Also, at a lower temperature, insufficient thermal energy does not allow the carriers to excite into higher states. So, the observed red
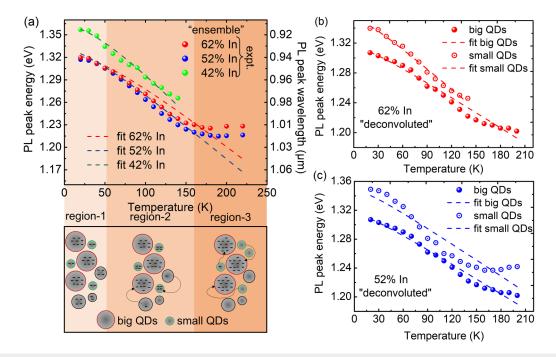
FIG. 4. (a) PL peak emission energy as a function of temperature along with the Varshni fitting for the three QD samples with 62%, 52%, and 42% In contents. Three distinct regions are identified in the plot and the thermal carrier transfer among QDs of different size is modeled for each region. Individual fitting for small and big QD family in the samples with In contents of (b) 62% and (c) 52% is also shown.

shift of the PL peak position with increasing temperature in region-1 is very slim. In region-2 with the temperature range of 50–160 K, the red-shift is comparatively faster than region-1. The carriers in this temperature range are thermalized to higher QD energy states and thermal escape of carriers from QDs occurs. Here, QDs are distributed in a bi-modal manner as seen in AFM images in Fig. 2 and the histograms, where one/two specific family is dominant at a particular temperature.[21,22] At low temperatures, the carriers are homogeneously distributed to QDs of different shapes and sizes, but with increasing temperature, the outgoing carriers escape and get into dominant QD families. At a higher temperature, the excited states of that specific QD families begin to be filled and the emission characteristics of those dominant QD families are reflected through the ensemble PL spectra. Though a blueshift was supposed to be seen due to radiative transition from higher energy states, this effect is suppressed by the bandgap shrinkage due to increased lattice vibrations at elevated temperatures, and eventually, we see a continuous red shift of emission wavelengths.[35,36]

With further increasing temperature beyond region-2, a constant PL peak position is seen. It is assumed that the overflow of carriers from smaller QD family is faster than big QDs and entering after this range big QD family is the only contributing member toward radiative transition. As the energy states are closer in the big QD ensemble than the smaller ones, the change in PL peak position with temperature is not so pronounced at this region. Hence, we see a constant value of the optical transition energy. It

should be noted that the 42% In-containing sample exhibits an almost 2D-like morphology, poor carrier confinement due to higher dimensionality results in obtaining the PL signal only up to 160 K. The PL peak energy dependence with temperature for each QD sample is then attempted to fit with the empirical Varshni equation that is often used to model the temperature dependence of the bandgap in bulk semiconductors.[37] The measured data in the two samples with 62% and 52% In-content exhibit significant deviation from the fit. Hence, the observed exotic dependence of the PL peak positions with temperature in QD samples cannot be described by the Varshni equation, which is more appropriate for 3D-bulk structures. In the 42% In-containing sample, QDs were not formed, i.e., a planar 2D-like morphology was obtained instead. Due to weaker carrier confinement in thin film-like structures, PL signals were not obtained in the temperature range of >160 K, which result in the better fit with the Varshni equation. In other words, the monotonic dependence of the PL peak energy on the temperature in the 42% sample appears to be an artifact of the fitting. As can be understood from Fig. 4(a), the measured PL data in region-3 are what differ from the Varshni equation in both 52% and 62% samples. The carrier transfer mechanism is schematically shown on the bottom of Fig. 4(a), where the homogenous distribution of carrier in region-1 followed by carrier occupancy in the dominant family (region-2), and finally, the transfer of carriers from small- to big QDs (region-3) is seen.

After extracting transition energies from the deconvoluted PL spectra for 62% and 52% In-containing samples, Varshni fitting

was performed for each QD family. The PL peak energies of both the QD families of each sample at different temperatures are shown in Figs. 4(b) and 4(c). As there are geometric non-uniformities in the QD ensemble, some anomalies in the measured data are observed for QD families, leading to the moderate Varshni fits. Compared to the small QD family of the 62% sample, the Varshni fitting is poorer in the same family of the 52% sample, which might be due to the higher size inhomogeneity. As can be seen in Table I, there is a larger standard deviation of the QD size distribution for the 52% small QD family. It should be noted that the blue-shifting phenomenon is observed for the small QD family of the 52% sample at higher temperatures. This behavior is attributed to the occupation of carriers at higher energy states of small QD families. Even after carrier transfer to big QDs, a handsome number of carriers stay in small QDs. Radiative transitions from the higher energy states of the small QDs are expected to dominate over the lattice heating-induced bandgap shrinkage that causes a redshift. Also, as the contribution of small QDs in the 62% sample was found negligible at higher temperatures, the fitting was limited to region-2. Thus, the individual fitting of different QD families of varying In-contents expresses the significance of each family

toward the Varshni fitting of the entire QD ensemble and the reasons for deviation from the fitting.

To substantiate assumptions of TDPL emission, the FWHM of the QD ensembles at each temperature was also extracted. The TDPL-FWHM for all the three samples is shown in Fig. 5(a). In the low-temperature range (region-1), the FWHM decreases with increasing temperature and attains a minimum value at a certain temperature for each sample. At lower temperature, the dominant PL transition is a result of inhomogeneous distribution of different QD sizes and the combined contribution of ground state emission of each QD toward the PL spectra broadens the FWHM. With increasing temperature, the thermally activated carriers relax to the potential minima where the emission with the narrowest FWHM is recorded. After the lowest point, a transition to increasing FWHM is observed with increasing temperature. This behavior can be attributed to the enhanced electron–phonon scattering, being a dominant mechanism at high temperature, assumed for region-3 in Fig. 4. For 62% and 52% samples, the transition temperature T_f is recorded around 100 and 125 K, respectively. For the 42% In sample, a FWHM minimum of 45 meV is seen at 80 K, characteristic of a QW-like behavior.[24]
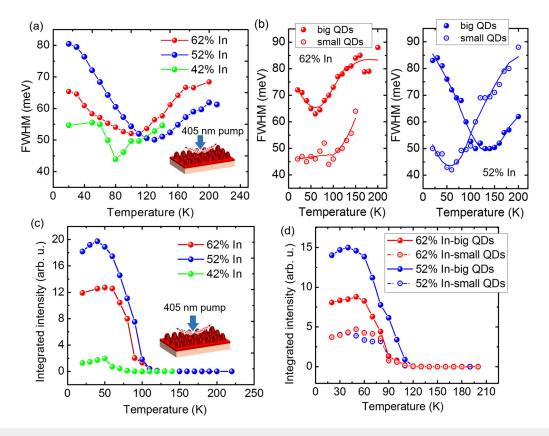

FIG. 5. (a) Variation of measured PL FWHMs with temperature for all the three QD samples, (b) FWHMs of the individual QD families extracted from the deconvoluted spectra for only 62% and 52% samples, (c) variation of integrated PL intensity for all the three QD samples with temperature, and (d) temperature-dependent integrated PL intensity of individual QD families for only 62% and 52% samples.
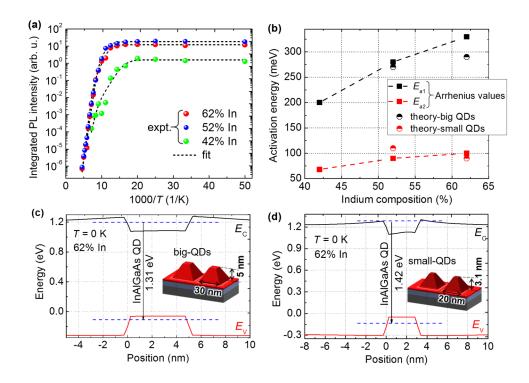
FIG. 6. (a) Integrated PL intensity as a function of 1000/T, fitting of Arrhenius equation (dotted line) is done on experimental data to extract activation energy, (b) Arrhenius vs calculated activation energy values with different indium compositions, and (c) and (d) band diagrams of only the 62% In sample to calculate the activation energy for big and small QDs, respectively.

The individual contributions of certain QD families toward the entire PL-FWHMs are shown in Fig. 5(b). It is seen that the big- and small QD families of both the 62% and 52% samples exhibit T_f at distinct temperatures. For the 62% sample, the difference in size for the small and big QDs is less pronounced as shown in the histograms of Figs. 2(d) and 2(e). As a result, nearly same carrier dynamics are observed for the big and small QD families and T_f occurs almost at the same temperature. On the other hand, T_f of the 52% sample occurs at separate temperatures, i.e., 60 and 130 K, for small and big QD families, respectively. This large difference of transition temperatures for big and small QD families is attributed to their noticeable differences in QD size. Compared to the 62% sample, there is a larger size deviation between the big- and small-QDs of the 52% In sample [see Figs. 2(b), 2(f), and 2(g)]. Due to the smaller size, it is assumed that carriers relax quickly to the ground state for the smaller QD family. T_f is, thus, seen at a lower temperature. The larger QDs in the 52% sample are expected to accommodate a larger number of carriers. Consequently, the carrier relaxation process is slowed down and T_f occurs at a higher temperature.

Calculation of the integrated PL intensity is another way to emphasize our interpretation on the TDPL behavior of the QD ensemble as shown in Fig. 5(c). An unusual behavior can be seen in the low temperature range, where the integrated PL intensity rises with increasing temperature followed by rapid degradation at elevated temperature. In the low-temperature regime, we attribute this behavior to thermal activation of trapped carriers into QD ground states, enhancing the total intensity of the PL signal and reaching an apex. At high temperature, augmented thermal energy forces the carriers out of the QD region falling into the barrier,

from where a non-radiative recombination takes place reducing the PL signal. As the temperature further increases and reach region-3, electron–phonon scattering becomes the superior mechanism. While the carriers in QDs continue to get more thermal energy, some carriers overflow into the GaAs barrier region from where they relax via non-radiative transition. This is assumed to be the primary cause for loss of the PL signal at elevated temperature (Fig. 3). The integrated intensity for each QD family extracted from the deconvoluted spectra is plotted in Fig. 5(d). At very low and high temperatures, the contribution of big QD family is found to be dominant, as described by the multi-Gaussian study.

As the lattice mismatch is the key factor in S-K grown QDs, another contributing factor might be the presence of defects in the interface of QD and the barrier layer, which explains the rapid degradation of the PL signal at higher temperature.[24,38] This is evidenced by the higher integrated PL intensity in the 52% sample compared to the 62% one with a larger lattice mismatch. For the 42% In-containing sample with the least lattice mismatch, a higher critical thickness does not result in 3D growth transition in our experiment. Hence, the carriers are then confined in only one direction that explains the low PL emission intensity.

For a deeper investigation of PL signal degradation at high temperature, thermal activation energy of the carriers in QDs was calculated using the Arrhenius equation,

$$I(T) = \frac{I_o}{1 + \sum_{a=1}^{i} \exp\left(-\frac{E_a}{k_B T}\right)}, \quad (1)$$

where I_o is the integrated PL intensity of the QD ensemble at $T = 0$ K, i are the energy states related to the localized states in the QD ensemble, and E_a is the thermal activation energy. Integrated PL intensity as a function of $1000/T$ is plotted in Fig. 6(a), and the experimental data are fit to Eq. (1). In our case, the best fits were obtained with two activation energies for all the three QD samples. Both activation energies as a function of In-content are plotted in Fig. 6(b). The presence of two different activation energies could be possibly attributed to the bimodal distribution of QDs. From the data presented in Fig. 6(a), higher activation energies E_{a1} are found to be 330, 280, and 200 meV for the samples with $x = 0.62$, 0.52, and 0.42, respectively. The extracted smaller activation energies E_{a2} are 100, 90, and 68 meV for the same set of samples. As expected, the smaller QDs have a lower activation energy compared to the bigger ones.[24] For the sample with 42% In content, the prediction of two QD families is not valid. But it is assumed that due to the non-homogeneity of the surface as well as variation of Al composition on the active layer accounts for spatial variation of bandgap give rise to localized states from where two different activation processes take place.

From Fig. 6(a), we see that E_{a1}, originating from the bigger QDs, is the dominant activation energy for temperature above 70 K, while for lower temperature, E_{a2} is the superior factor that arises from smaller QDs. This confirms the general interpretation that smaller QDs thermally activate at a lower temperature than the larger QDs. We assume that E_{a2} is related to the thermal repopulation of carriers in smaller QDs. Upon thermal activation, they repopulate to a larger QD family. While E_{a1} is more relevant toward the degradation of PL intensity at higher temperature, as the escape of carriers from larger QDs results in non-radiative recombination from GaAs barrier layers.

To draw a conclusion of PL-intensity degradation with the thermal activation of carriers, the energy eigenstates of the QDs samples were calculated. For simulation, two representative QDs from the big- and small-families were chosen with mean height and diameter listed in Table I for each composition. A 6-band $k.p$ model was employed for the simulation. As the contribution of electron–hole Coulomb interaction was negligible (<5 meV), this was not considered in the simulation. Band diagrams with first energy-states are plotted for the 62% In-containing sample in Figs. 6(c) and 6(d) for big and small QDs, respectively. The difference between PL emission energy and the barrier bandgap energy of QDs as a function of indium contents is plotted in Fig. 6(b) and compared with calculated activation energies E_{a1} and E_{a2}. The energy differences of the big and small QDs are found to be close to activation energies calculated for each family, thus confirming our assumptions on carrier repopulation as well as rapid degradation of the PL signal at higher temperatures.

CONCLUSION

This work experimentally investigates the TDPL spectroscopic behavior of InAlGaAs/GaAs QDs with three different indium compositions. All the anomalies in the TDPL behavior are fitted with theory and understood in detail. As the TDPL characteristics are reflected in QD-based device performance, this study suggests the stable operation window and predicts any temperature behavior of the QDs once integrated into active devices. Quaternary InAlGaAs QDs are particularly important for shorter wavelength device applications with enhanced thermal stability. *Ex situ* techniques such as rapid thermal annealing (RTA) are a potential way to improve QD homogeneity in the ensemble.[34,39] Also, modulation *p*-doping near the active region has emerged to be an effective way for thermal stability for some other QD-based devices and materials,[40] paving the way to next-generation temperature stable QD devices operating at shorter wavelengths.

AUTHOR DECLARATIONS

Conflict of Interest

The authors have no conflicts to disclose.

Author Contributions

S.L. and R.A. contributed equally to this work.

DATA AVAILABILITY

The data that support the findings of this study are available from the corresponding author upon reasonable request.

REFERENCES

[1]S. Chen, M. Tang, Q. Jiang, J. Wu, V. G. Dorogan, M. Benamara, Y. I. Mazur, G. J. Salamo, P. Smowton, and A. Seeds, "Inas/GaAs quantum-dot superluminescent light-emitting diode monolithically grown on a Si substrate," ACS Photonics **1**, 638 (2014).

[2]N. N. Ledentsov, V. M. Ustinov, V. A. Shchukin, P. S. Kop'Ev, Z. I. Alferov, and D. Bimberg, "Quantum dot heterostructures: Fabrication, properties, lasers," Semiconductors **32**, 343 (1998).

[3]S. Krishna, "Quantum dots-in-a-well infrared photodetectors," J. Phys. D: Appl. Phys. **38**, 2142 (2005).

[4]J. Claudon, J. Bleuse, N. S. Malik, M. Bazin, P. Jaffrennou, N. Gregersen, C. Sauvan, P. Lalanne, and J.-M. Gérard, "A highly efficient single-photon source based on a quantum dot in a photonic nanowire," Nat. Photonics **4**, 174 (2010).

[5]A. Abdollahinia, S. Banyoudeh, A. Rippien, F. Schnabel, O. Eyal, I. Cestier, I. Kalifa, E. Mentovich, G. Eisenstein, and J. P. Reithmaier, "Temperature stability of static and dynamic properties of 1.55 μm quantum dot lasers," Opt. Express **26**, 6056 (2018).

[6]H. Huang, J. Duan, D. Jung, A. Y. Liu, Z. Zhang, J. Norman, J. E. Bowers, and F. Grillot, "Analysis of the optical feedback dynamics in InAs/GaAs quantum dot lasers directly grown on silicon," J. Opt. Soc. Am. B **35**, 2780 (2018).

[7]T. Septon, A. Becker, S. Gosh, G. Shtendel, V. Sichkovskyi, F. Schnabel, A. Sengül, M. Bjelica, B. Witzigmann, and J. P. Reithmaier, "Large linewidth reduction in semiconductor lasers based on atom-like gain material," Optica **6**, 1071 (2019).

[8]D. L. Huffaker, G. Park, Z. Zou, O. B. Shchekin, and D. G. Deppe, "1.3 μm room-temperature GaAs-based quantum-dot laser," Appl. Phys. Lett. **73**, 2564 (1998).

[9]S. Banyoudeh, A. Abdollahinia, O. Eyal, F. Schnabel, V. Sichkovskyi, G. Eisenstein, and J. P. Reithmaier, "Temperature-insensitive high-speed directly modulated 1.55-μm quantum dot lasers," IEEE Photonics Technol. Lett. **28**, 2451 (2016).

[10]S. Hasan, O. Richard, C. Merckling, and W. Vandervorst, "Encapsulation study of MOVPE grown InAs QDs by InP towards 1550 nm emission," J. Cryst. Growth **557**, 126010 (2021).

[11]A. Knigge, A. Klehr, H. Wenzel, A. Zeghuzi, J. Fricke, A. Maaßdorf, A. Liero, and G. Tränkle, "Wavelength-stabilized high-pulse-power laser diodes for automotive LiDAR," Phys. Status Solidi A **215**, 1700439 (2018).

[12]T. W. Schlereth, C. Schneider, W. Kaiser, S. Höfling, and A. Forchel, "Low threshold, high gain AlGaInAs quantum dot lasers," Appl. Phys. Lett. **90**, 221113 (2007).

[13]H. G. Mahran and K. M. Drbala, "Efficacy of twelve sessions of 905 nm infrared laser on acne vulgaris," Ann. Clin. Anal. Med. **11**, 191 (2020).

[14]W. Challener, C. Peng, A. Itagi, D. Karns, W. Peng, Y. Peng, X. Yang, X. Zhu, N. Gokemeijer, and Y.-T. Hsia, "Heat-assisted magnetic recording by a near-field transducer with efficient optical energy transfer," Nat. Photonics **3**, 220 (2009).

[15]S. Fafard, S. Raymond, G. Wang, R. Leon, D. Leonard, S. Charbonneau, J. L. Merz, P. M. Petroff, and J. E. Bowers, "Temperature effects on the radiative recombination in self-assembled quantum dots," Surf. Sci. **361-362**, 778 (1996).

[16]T. W. Schlereth, C. Schneider, S. Gerhard, S. Hofling, and A. Forchel, "Short-wavelength (760–920 nm) AlGaInAs quantum dot lasers," IEEE J. Sel. Top. Quantum Electron. **15**, 792 (2009).

[17]D. L. Huffaker, L. A. Graham, and D. G. Deppe, "Low-threshold continuous-wave operation of an oxide-confined vertical cavity surface emitting laser based on a quantum dot active region and half-wave cavity," Electron. Lett. **33**, 1225 (1997).

[18]O. Baklenov, D. L. Huffaker, A. Anselm, D. G. Deppe, and B. G. Streetman, "Influence of Al content on formation of InAlGaAs quantum dots grown by molecular beam epitaxy," J. Appl. Phys. **82**, 6362 (1997).

[19]Y. Horikoshi, H. Yamaguchi, F. Briones, and M. Kawashima, "Growth process of III–V compound semiconductors by migration-enhanced epitaxy," J. Cryst. Growth **105**, 326 (1990).

[20]R. Arefin, S. Lee, H. Jung, J. Ha, J. S. Kim, S. Krishna, and S. Arafin, "MBE growth and characterization of InAlGaAs/GaAs quantum dots 2021," in *IEEE Research and Applications of Photonics in Defense Conference (RAPID), Virtual* (IEEE, 2021), pp. 1–2.

[21]H. L. Wang, D. Ning, and S. L. Feng, "Temperature dependence of the optical properties of InAs/GaAs self-organized quantum dots with bimodal size distribution," J. Cryst. Growth **209**, 630 (2000).

[22]Y. C. Zhang, C. J. Huang, F. Q. Liu, B. Xu, J. Wu, Y. Chen, J. Ding, W. H. Jiang, X. L. Ye, and Z. G. Wang, "Thermal redistribution of photocarriers between bimodal quantum dots," J. Appl. Phys. **90**, 1973 (2001).

[23]G. Muñoz-Matutano, I. Suárez, J. Canet-Ferrer, B. Alén, D. Rivas, L. Seravalli, G. Trevisi, P. Frigeri, and J. Martínez-Pastor, "Size dependent carrier thermal escape and transfer in bimodally distributed self assembled InAs/GaAs quantum dots," J. Appl. Phys. **111**, 123522 (2012).

[24]Y. T. Dai, J. C. Fan, Y. F. Chen, R. M. Lin, S. C. Lee, and H. H. Lin, "Temperature dependence of photoluminescence spectra in InAs/GaAs quantum dot superlattices with large thicknesses," J. Appl. Phys. **82**, 4489 (1997).

[25]S. Lee, H. J. Jo, S. Mathews, J. A. Simon, T. J. Ronningen, S. H. Kodati, D. R. Fink, J. S. Kim, M. Winslow, and C. H. Grein, "Investigation of carrier localization in InAs/AlSb type-II superlattice material system," Appl. Phys. Lett. **115**, 211601 (2019).

[26]T. Finke, V. Sichkovskyi, and J. P. Reithmaier, "Optimization of size uniformity and dot density of $In_xGa_{1-x}As$/GaAs quantum dots for laser applications in 1 μm wavelength range," J. Cryst. Growth **517**, 1 (2019).

[27]T. J. Krzyzewski, P. B. Joyce, G. R. Bell, and T. S. Jones, "Scaling behavior in InAs/GaAs (001) quantum-dot formation," Phys. Rev. B **66**, 201302 (2002).

[28]S. Birner, T. Zibold, T. Andlauer, T. Kubis, M. Sabathil, A. Trellakis, and P. Vogl, "Nextnano: General purpose 3-D simulations," IEEE Trans. Electron Devices **54**, 2137 (2007).

[29]K. Pierz, Z. Ma, U. F. Keyser, and R. J. Haug, "Kinetically limited quantum dot formation on AlAs (1 0 0) surfaces," J. Cryst. Growth **249**, 477 (2003).

[30]E. M. Pavelescu, C. Gilfert, J. Reithmaier, A. Martin-Minguez, and I. Esquivias, "GaInAs/(Al) GaAs quantum-dot lasers with high wavelength stability," Semicond. Sci. Technol. **23**, 085022 (2008).

[31]L. Brusaferri, S. Sanguinetti, E. Grilli, M. Guzzi, A. Bignazzi, F. Bogani, L. Carraresi, M. Colocci, A. Bosacchi, and P. Frigeri, "Thermally activated carrier transfer and luminescence line shape in self-organized InAs quantum dots," Appl. Phys. Lett. **69**, 3354 (1996).

[32]H. Lee, W. Yang, and P. C. Sercel, "Temperature and excitation dependence of photoluminescence line shape in InAs/GaAs quantum-dot structures," Phys. Rev. B **55**, 9757 (1997).

[33]S. Bauer, V. Sichkovskyi, and J. P. Reithmaier, "Growth and optical characteristics of InAs quantum dot structures with tunnel injection quantum wells for 1.55 μm high-speed lasers," J. Cryst. Growth **491**, 20 (2018).

[34]S. Bauer, V. Sichkovskyi, F. Schnabel, A. Sengül, and J. P. Reithmaier, "Comparison between InP-based quantum dot lasers with and without tunnel injection quantum well and the impact of rapid thermal annealing," J. Cryst. Growth **516**, 34 (2019).

[35]P. Zhou, X. Zhang, X. Liu, J. Xu, and L. Li, "Temperature-dependent photoluminescence properties of quaternary ZnAgInS quantum dots," Opt. Express **24**, 19506 (2016).

[36]J. Piprek, *Semiconductor Optoelectronic Devices* (Academic, Oxford, 2003), p. 20.

[37]Y. P. Varshni, "Temperature dependence of the energy gap in semiconductors," Physica **34**, 149 (1967).

[38]H. Y. Liu, S. L. Liew, T. Badcock, D. J. Mowbray, M. S. Skolnick, S. K. Ray, T. L. Choi, K. M. Groom, B. Stevens, F. Hasbullah, C. Y. Jin, M. Hopkinson, and R. A. Hogg, "p-doped 1.3 μm InAs/GaAs quantum-dot laser with a low threshold current density and high differential efficiency," Appl. Phys. Lett. **89**, 073113 (2006).

[39]S. Sanguinetti, T. Mano, A. Gerosa, C. Somaschini, S. Bietti, N. Koguchi, E. Grilli, M. Guzzi, M. Gurioli, and M. Abbarchi, "Rapid thermal annealing effects on self-assembled quantum dot and quantum ring structures," J. Appl. Phys. **104**, 113519 (2008).

[40]Q. Li, X. Wang, Z. Zhang, H. Chen, Y. Huang, C. Hou, J. Wang, R. Zhang, J. Ning, and J. Min, "Development of modulation p-doped 1310 nm InAs/GaAs quantum dot laser materials and ultrashort cavity Fabry–Perot and distributed-feedback laser diodes," ACS Photonics **5**, 1084 (2018).